HHS Public Access

Author manuscript

Magn Reson Med. Author manuscript; available in PMC 2019 February 01.

Published in final edited form as:

Magn Reson Med. 2018 February ; 79(2): 826–838. doi:10.1002/mrm.26745.

Five-Dimensional Whole-Heart Sparse MRI

Li Feng[1,*,‡], **Simone Coppo**[2,3,‡], **Davide Piccini**[2,4], **Jerome Yerly**[2,3], **Ruth P Lim**[5], **Pier Giorgio Masci**[6], **Matthias Stuber**[2,3], **Daniel K. Sodickson**[1], and **Ricardo Otazo**[1]

[1]Center for Advanced Imaging Innovation and Research (CAI2R), and Bernard and Irene Schwartz Center for Biomedical Imaging, Department of Radiology, New York University School of Medicine, New York, NY, United States [2]Department of Radiology, University Hospital (CHUV) and University of Lausanne (UNIL), Lausanne, Switzerland [3]Center for Biomedical Imaging (CIBM), Lausanne, Switzerland [4]Advanced Clinical Imaging Technology, Siemens Healthcare, Lausanne, Switzerland [5]Department of Radiology, Austin Health and The University of Melbourne, Melbourne, Victoria, Australia [6]Division of Cardiology and Cardiac MR Center, University Hospital (CHUV),Lausanne, Switzerland

Abstract

Purpose—A five-dimensional (5D) whole-heart sparse imaging framework is proposed for simultaneous assessment of myocardial function and high-resolution cardiac and respiratory motion-resolved whole-heart anatomy in a single continuous non-contrast MR scan.

Methods—A non-ECG-triggered 3D golden-angle radial b-SSFP sequence was employed for data acquisition. The acquired 3D k-space data were sorted into a 5D dataset containing separated cardiac and respiratory dimensions using a self-extracted respiratory motion signal and a recorded ECG signal. Images were then reconstructed using XD-GRASP, a multidimensional compressed sensing technique exploiting correlations/sparsity along cardiac and respiratory dimensions. 5D whole-heart imaging was compared with respiratory motion-corrected 3D and 4D whole-heart imaging in nine volunteers for evaluation of the myocardium, great vessels and coronary arteries. It was also compared to breath-held, ECG-gated 2D cardiac cine imaging for validation of cardiac function quantification.

Results—5D whole-heart images received systematic higher quality scores in the myocardium, great vessels and coronary arteries. Quantitative coronary sharpness and length were always better for the 5D images. Good agreement was obtained for quantification of cardiac function compared to 2D cine imaging.

Conclusion—Five-dimensional whole-heart sparse imaging represents a robust and promising framework for simplified comprehensive cardiac MRI without the need for breath-hold and motion correction.

Address correspondence to: Li Feng, PhD, Center for Advanced Imaging Innovation and Research (CAI^{2}R), Department of Radiology, New York University School of Medicine, 660 First Ave, New York, NY 10016, Phone : 212-263-0409, Fax : 212-263-7541, Li.Feng@nyumc.org.

‡Li Feng and Simone Coppo contributed equally to this study.

Keywords

whole-heart MRI; compressed sensing; 3D radial sampling; golden-angle; coronary MRA; respiratory motion

Introduction

Cardiac MRI, particularly imaging of small vessels such as the coronary arteries, remains a challenging task (1–3). Major challenges include: **i)** motion of the heart during the cardiac and respiratory cycles, **ii)** the complexity of cardiovascular anatomy, and **iii)** limitations related to comparatively slow imaging speed. These factors have led to a complex and time-consuming clinical workflow for traditional cardiac imaging, in which a series of 2D imaging acquisitions are employed during multiple breath-holds (4–7). These acquisitions must be individually tailored and adjusted, in a manner that is highly dependent on operator experience and on patients' ability and capacity to hold their breath.

3D cardiac MRI can overcome some of the abovementioned problems and is an attractive alternative to conventional tailored 2D scans. 3D cardiac imaging can provide comprehensive information with minimum scan planning, allowing a multifaceted assessment of the cardiovascular system (8–11). It offers increased signal-to-noise ratio, large spatial coverage, and the ability to reconstruct images in any desired orientation. However, a major challenge associated with 3D data acquisition is comparatively long scan time, which makes it difficult to meet competing demands of spatial resolution, temporal resolution and volumetric coverage. 3D acquisition also requires reliable cardiac and respiratory motion compensation strategies to avoid image blurring. For the coronary arteries, a 3D cardiac scan must also provide good vessel contrast, in order to discriminate arteries from surrounding epicardial fat and myocardium (3,12). Due to these limitations, 3D cardiac MRI is currently limited to a subset of specific applications in routine clinical setting such as MR angiography (MRA).

During the past decade, a variety of four-dimensional (4D) cardiac MRI techniques have been proposed (13–23), where time-resolved 3D volumes are acquired covering the entire cardiac cycle. 4D MRI allows cardiac motion-resolved reconstruction and does not require setup of ECG trigger delay times. However, respiratory motion still remains a challenge. Existing strategies to handle respiratory motion in 4D cardiac MRI can be roughly divided into two categories. In the first category, "gating" is usually performed using motion signals extracted from external devices such as respiratory bellows or intrinsically acquired self-navigator (18,23). Despite its simple implementation and robust performance, such approaches suffer from reduced scan efficiency, since only part of the data acquired in a specific temporal window (e.g., end-expiration) is used to reconstruct final images. The second category aims at improving the scan efficiency by combining images at different respiratory phases using an image registration algorithm, which models the movement of heart during respiration as translation (24–29), affine (20,30–34) or non-rigid (35) transformation.

Recently, a different approach for handling respiratory motion called eXtra-Dimensional Golden-angle RAdial Sparse Parallel MRI (XD-GRASP) (36) has been proposed. Instead of either removing or correcting for motion, XD-GRASP sorts the acquired data into multiple undersampled motion states and then reconstructs them as a multidimensional image series with full information. This approach does not rely on assumptions about motion models (e.g., translation, affine, or non-rigid) as in registration-based correction methods, maintains high scan efficiency, and provides access to additional physiologic information of potential clinical value (37). Successful applications of XD-GRASP have been demonstrated for free-breathing liver MRI (36,38), whole-heart coronary MRA (39) and cardiac cine MRI (36,40,41).

The purpose of this work is to extend the idea of XD-GRASP for 4D whole-heart imaging to reconstruct a 5D motion-resolved image series and test the framework in a first proof-of-concept volunteer study. The five dimensions in this framework include the three spatial dimensions (x-y-z) plus two distinct temporal dimensions representing cardiac and respiratory phases, respectively. The proposed framework was compared against 3D and 4D whole-heart imaging approaches for assessment of the myocardium, great vessels and coronary arteries. It was also compared to breath-held, ECG-gated multislice 2D cardiac cine imaging for validation of cardiac function quantification.

Methods

5D Whole-Heart Sparse MRI Framework

Components of the proposed framework, including pulse sequence, sampling scheme, motion extraction and image reconstruction are described in this section.

Pulse Sequence—A prototype free-running non-ECG-triggered 3D golden-angle radial balanced steady-state free precession (b-SSFP) sequence (22) that was based on a previously proposed whole-heart coronary MRA approach (25,42) is employed for continuous whole-heart MR data acquisitions covering a large number of cardiac cycles. The 3D radial sampling scheme, as shown in Figure 1a&b, is segmented into multiple interleaves based on the spiral phyllotaxis pattern (42), in which each interleave is rotated by the golden-angle about the z-axis with respect to the previous interleave. Each interleave starts with a readout oriented along the superior-to-inferior (SI) direction for respiratory self-navigation (24) and is preceded by fat saturation. Because the steady-state is periodically interrupted by fat saturation pulses (~25ms duration), additional ten linearly increasing start-up angles (LISA) RF pulses, which are also known as ramp-up pulses, are inserted before the data acquisition in each interleave. The golden-angle sampling scheme enables continuous k-space coverage without the need to predefine cardiac phases within the acquisition protocol. When compared against a conventional ECG-triggered data acquisition, the continuous sampling strategy not only eliminates the need for setup of ECG trigger delay times, but also enables simultaneous assessment of myocardial function and the whole-heart anatomy at different cardiac phases.

Motion Extraction—Reliable respiratory and cardiac motion signals are needed to sort the acquired data. The self-navigation k-space profiles acquired at the beginning of each

interleave (red lines in Figure 1b) can be used to extract respiratory motion signal using a principal component analysis (PCA) approach that was previously validated for whole-heart MRI (20) and DCE-MRI (36,38). Specifically, a 1D partition-direction fast Fourier transform (FFT) is performed on these self-navigation profiles (thus obtaining a series of SI projections of the whole volume), followed by PCA along the concatenated z+coil dimension to determine the most common signal variation mode. A principal component with the highest ratio between its peak in the respiratory motion frequency range (0.1–0.5Hz) and its peak in the cardiac motion frequency range (0.5–1.5Hz) is selected to represent the respiratory motion signal. Figure 1c shows a representative respiratory motion signal that is superimposed on an example series of SI projections. The cardiac motion signal is extracted retrospectively from the recorded ECG time stamps that are synchronized with data acquisitions as described in (22).

Data Sorting—Given the extracted respiratory and cardiac motion signals, the series of continuously acquired 3D radial lines can be sorted into a 5D dataset (k_x-k_y-k_z-cardiac-respiratory) as shown in Figure 2. Specifically, the series of 3D radial lines is first binned into different cardiac phases with a desired temporal resolution using the cardiac motion signal, and each cardiac phase is further sorted into multiple respiratory phases spanning from end-expiration to end-inspiration using the estimated respiratory motion signal. The data sorting process is performed such that the number of spokes grouped in each temporal frame is the same, as performed in our prior XD-GRASP works (36,39).

XD-GRASP Reconstruction—5D image reconstruction is performed by solving the following optimization problem that enforces **i)** sparsity along both cardiac and respiratory dimensions and **ii)** multicoil data consistency:

$$m=\arg\min_{m}\|F\cdot C\cdot m-d\|_2^2+\lambda_c\|D_c\cdot m\|_1+\lambda_r\|D_r\cdot m\|_1 \quad [1]$$

Here, F is the non-uniform FFT (NUFFT), m is the 5D image (x-y-z-cardiac-respiratory) to be reconstructed, C is the estimated coil sensitivities and d is the sorted k-space data (k_x-k_y-k_z-cardiac-respiratory-coil). D_c and D_r are the first-order differences (difference between consecutive frames) along the sorted cardiac dimension and respiratory dimension, respectively. These differences are employed as sparsifying transforms to exploit cardiac and respiratory correlations and thus to reconstruct the undersampled multidimensional data. λ_c and λ_c are corresponding regularization weights that control the tradeoff between data consistency and sparsity constraints.

Data Acquisition

Imaging was performed in nine healthy volunteers (age=28±4 years, 5 males) at the University of Lausanne and was approved by the Institutional Review Board. Written informed consent was obtained from all subjects before MR scans. Three types of MR scans were performed in all subjects on a 1.5T MR scanner (MAGNETOM Aera, Siemens Healthcare, Erlangen, Germany) without contrast injection, including **i)** free-breathing non-ECG-triggered whole-heart MRI, **ii)** free-breathing ECG-triggered and self-navigated

whole-heart MRI, and **iii)** breath-held, ECG-gated multislice 2D cardiac cine MRI. In addition, conventional ECG-triggered and navigator-gated free-breathing 3D Cartesian whole-heart MRI was also performed in two subjects in two separate visits and this was included for visual comparison only.

Free-Breathing Non-ECG-Triggered Whole-Heart MRI—Free-breathing non-ECG-triggered whole-heart MRI was performed using the sequence described in the "*Pulse Sequence*" section (22). Relevant imaging parameters included: TR/TE = 3.1/1.56 ms, FOV = 220 mm^3, matrix size = 192^3, voxel size = 1.15 mm^3, and flip angle = 90°. Data acquisition featured non-slice-selective RF pulses and a total number of 126478 spokes were acquired in each subject in 14 minutes and 17 seconds, including 5749 golden-angle-rotated interleaves with 22 spokes each. Each interleave was preceded by a CHESS fat saturation pulse and ten ramp-up RF pulses. The average specific absorption rate (SAR) of the scans was ~97% of the SAR limit in the "first level" mode (4 W/kg, as defined in the international standard IEC 60601-2-33).

Free-Breathing ECG-Triggered and Self-Navigated Whole-Heart MRI—Free-breathing ECG-triggered whole-heart *MRI* was performed using a prototype 3D radial b-SSFP sequence with the same spiral phyllotaxis golden-angle rotation scheme, which was previously tested in both volunteer and patient studies (25,27,43). Data acquisition was performed without respiratory gating, and the acquisition window was placed at the mid-diastolic phase to minimize cardiac motion-induced effects. Relevant imaging parameters included: TR/TE = 3.1/1.56ms, FOV = 220 mm^3, matrix size = 192^3, voxel size = 1.15 mm^3 and flip angle = 115°. Data acquisition featured non-slice-selective RF pulses and a total number of 12064 spokes were acquired in each subject, including 377 interleaves with 32 spokes each. Each interleave was preceded by a T_2 preparation module, a CHESS fat saturation pulse and ten ramp-up RF pulses. Each interleave started with a spoke oriented along the SI direction for self-navigation. The scan time was 377 heart-beats long, and, thus, it was dependent on the heart rate of each subject.

Free-Breathing ECG-Triggered and Navigator-Gated Whole-Heart MRI—Free-breathing ECG-triggered and navigator-gated whole-heart MRI was performed using a 3D b-SSFP Cartesian imaging protocol described by Sakuma H et al in (44). Key imaging parameters include: FOV = 280 × 280 × 120 mm^3, matrix size = 256 × 256 × 80, voxel size = 1.09 × 1.09 × 1.5 mm^3, number of segment = 35 and flip angle = 90°. Each segment was preceded by a T_2 preparation module, a CHESS fat saturation pulse and ten ramp-up RF pulses. The acceptance window for navigator-gating was ±2.0 mm. Data were acquired with a GRAPPA factor of 2 and the total scan time was dependent on respiratory pattern (one subject with 5:59 min and the other subject with 6:43 min). Image were reconstructed with half of the acquired voxel size (0.55 × 0.55 × 0.75 mm^3).

Multislice 2D Cardiac Cine MRI—Breath-held and retrospective ECG-gated multislice 2D cardiac cine MRI was performed in a short axis (SAX) orientation. Relevant imaging parameters included: TR/TE=3.06/1.28ms, voxel size = 1.2 × 1.2 mm^2, FOV = 300 × 171 mm^2, matrix size = 256 × 146, slice thickness = 8 mm and flip angle = 80°. A total of 12

slices were acquired in each subject covering the entire left ventricle and each slice was acquired during one breath-hold. Images were acquired and reconstructed with 25 cardiac phases with a GRAPPA factor of 2, resulting in a temporal resolution of under 50 ms. The scan time was 11:47 ± 2:32 min including the SAX scout scanning.

Image Reconstruction

5D Whole-Heart Sparse Image Reconstruction—The non-ECG-triggered whole-heart datasets were reconstructed using the 5D XD-GRASP reconstruction framework as described above. Specifically, each dataset was first sorted into 20 cardiac phases using the cardiac signal, generating an image series with temporal resolution of about 40–50 ms. The number of cardiac phases was selected such that the resulting temporal resolution was adequate for quantification of global cardiac function (45). In the next step, each cardiac phase was further sorted into four respiratory motion phases spanning from end-expiration to end-inspiration using the respiratory motion signal, thus generating a 5D dataset with a matrix size of 192×192×192×20×4. The number of respiratory phases was selected according to our prior experiences with XD-GRASP for motion-resolved DCE-MRI (36) and coronary MRA (39). In both studies, it was concluded that four respiratory phases were adequate to resolve respiratory motion.

The sorted 5D whole-heart images were reconstructed using a non-linear conjugate gradient algorithm (46,47). Coil sensitivity maps were calculated using the adaptive combination approach (48) and were estimated from a 3D image volume reconstructed using all the acquired k-space data. In order to speed up image reconstruction, the NUFFT operation was implemented using parallel computing in graphics processing units (GPUs) (49), and was called in the main reconstruction program implemented in MATLAB (Mathworks, MA). All reconstructions were performed in a server equipped with two 16-core CPUs, 256 GB RAM, and two 6-Gb NVIDIA GPU cards.

Based on our prior experience with sparse cardiac MRI, first-order differences for minimizing the total variation along the temporal dimensions were employed separately along the cardiac and respiratory dimensions. The corresponding regularization parameters were systematic evaluated and were empirically determined as previously performed in (39). In addition, quantitative measure of coronary sharpness was also compared in one representative dataset for a range of different values. The parameters that achieved the best combination of vessel sharpness and visual image quality were then empirically selected and then applied to all subsequent 5D image reconstructions.

4D Whole-Heart Sparse Image Reconstruction—For comparison, the same datasets used for 5D image reconstruction were also reconstructed using a respiratory motion-corrected GRASP (Golden-angle RAdial Sparse Parallel imaging) approach (47) with sparsity constraint along the cardiac motion dimension only (50). As described in (22,25), the respiratory motion signal was extracted by performing cross-correlation on the self-navigation projection, and the resulting 1D SI displacement was then used for correcting each data interleave before image reconstruction by directly applying an angle-specific phase shift to all k-space readouts (24). The respiratory motion-corrected k-space data were

then sorted into 20 cardiac phases and the 4D whole-heart images (192×192×192×20) were reconstructed using GRASP (47,50). The selection of regularization parameter was performed in the same manner as previously described for the XD-GRASP reconstruction.

Self-Navigated 3D Whole-Heart Image Reconstruction—The ECG-triggered and *self-navigated* 3D whole-heart datasets were reconstructed directly on the MR scanner using a 3D gridding algorithm. The respiratory motion detection and correction were the same as for the 4D sparse image reconstruction, with more details described in (25,27).

Image Analysis

Image Quality Assessment—For each subject, one end-systolic and one mid-diastolic cardiac phase were retrospectively selected from the 4D whole-heart and the end-expiratory phase of the 5D whole-heart image sets. All images, including the self-navigated 3D whole-heart images (diastole only) and the selected cardiac phases (one end-systole and one mid-diastole) of 4D and 5D whole-heart images, were pooled and randomized for blinded assessment. A radiologist (R.P.L.) and a cardiologist (P.G.M) with 11-years' and 10-years' experience in cardiovascular MRI scored the image quality of the myocardium, ascending aorta (Asc Aorta), descending aorta (Desc Aorta), main pulmonary artery (MPA), right pulmonary arteries (RPA), left pulmonary arteries (LPA) and superior vena cava (SVC) on a 0–4 scale as follows: 0 = non-diagnostic, 1 = poor, 2 = adequate, 3 = good, 4 = excellent. The same readers also scored the image quality of right coronary artery (RCA), left main coronary artery (LM) and left anterior descending coronary artery (LAD) on a 0–4 scale, which classified the definition of the vessel borders as follows: 0 = not visible, 1 = markedly blurred, 2 = moderately blurred, 3 = mildly blurred, and 4 = sharply defined. Any coronary artery with a grade higher than 0 was considered visible.

Quantitative Evaluation of Coronary Arteries—The vessel sharpness (conspicuity) of the proximal segment and mid segment of the RCA and LAD (51), as well as the visible vessel length of RCA and LM+LAD, were measured for the self-navigated 3D whole-heart images (diastole only) and the selected cardiac phases (one end-systole and one mid-diastole) of 4D and 5D whole-heart images. Soap-bubble software (52) was used for all coronary artery reformatting and quantitative measurement.

Evaluation of Cardiac Function—End-Systolic Volume (ESV), End-Diastolic Volume (EDV), and Ejection fraction (EF) were compared between the 5D whole heart images (end-expiratory phase) and the breath-held 2D cine images. For 5D images, quantification was performed using a tool developed in MATLAB. The end-systolic 3D volume when the myocardium reaches the maximal contraction and a diastolic 3D volume when the myocardium reached the maximal relaxation were visually selected and reformatted to the same orientation as corresponding 2D slices using orientation information extracted from the DICOM header of 2D images. The blood-myocardium boundary was then manually segmented in each slice of the selected 3D volume, and the left ventricular volume was calculated by multiplying the segmented left ventricular area (number of voxels) by the voxel volume (1.15 mm^3). The EF was calculated as

$$EF = \frac{EDV - ESV}{EDV} * 100 \quad [2]$$

For multislice 2D cardiac cine images, the cardiac function was measured using commercial Argus VF software (Syngo Argus, Siemens Medical Solutions, Germany). Validation of the 4D whole-heart imaging technique was previously reported (50) and thus it was not included in this study.

Statistical Analysis

A nonparametric paired two-tailed Wilcoxon signed-rank test was used to compare the reported image quality scores for 5D whole-heart v.s. 4D whole-heart in both diastole and systole and 5D whole-heart v.s. self-navigated 3D whole-heart in diastole. A *P* value smaller than 0.05 was considered statistically significant. For great vessels, the scores of different arteries were considered together for each imaging technique. For coronary arteries, the scores of different segments were considered together for each imaging technique. The inter-reader variability was assessed using Bland–Altman analysis.

A two-tailed paired Student's t-test was used to compare the measured coronary vessel sharpness and length on a per-vessel basis for 5D whole-heart v.s. 4D whole-heart in both diastole and systole and 5D whole-heart v.s. self-navigated 3D whole-heart in diastole. A *P* value smaller than 0.05 was considered statistically significant. Bland–Altman analysis was used to compare cardiac function measure between 5D whole-heart and 2D cine imaging.

Results

All images were reconstructed successfully. The average reconstruction time was 407.79 ± 18.86 min for the 5D whole-heart sparse images and was 173.53 ± 10.56 min for the 4D whole-heart sparse images.

Table 1a summarizes averaged reader scores for image quality of the myocardium and great vessels, and the sharpness of the coronary arteries. 5D whole-heart images achieved systematic higher scores than respiratory motion-corrected 4D and self-navigated 3D whole-heart images. The improvement reached statistical significance ($P<0.05$) in all assessments. Table 1b summarizes the measured coronary sharpness and vessel length. As was the case for the qualitative comparison, 5D whole-heart images achieved systematically improved sharpness. Statistical significance ($P<0.05$) was reached in all comparisons except for 5D v.s. 4D in the systolic RCA. For the measures of vessel length, significant improvement ($P<0.05$) was achieved for 5D v.s. self-navigated 3D in the diastolic RCA and 5D v.s. 4D in the systolic LM+LAD. The Bland-Altman plot of inter-reader variability is shown in the Supporting Materials (Figure S1). The mean score differences for the great vessels/myocardium and the coronary arteries were 0.3 and 0.4, respectively.

Figure 3 shows slices of the ventricular chambers and the aorta in end-expiration in one representative volunteer, derived from the 5D whole-heart images. Good delineation of the myocardial wall and aorta can be obtained in both diastolic and systolic phases. Figure 4

shows a comparison between 4D whole-heart images and 5D whole-heart images in coronal and sagittal planes from another volunteer. The white lines overlaid atop the diaphragm in the 5D whole-heart images demonstrate that respiratory motion can be resolved using the proposed method. A zoomed view of the myocardium from the same dataset is shown in Figure 5, where residual respiratory motion blurring can be found in the myocardium and papillary muscle of the 4D whole-heart images (white arrows).

Figure 6a shows a comparison of the myocardium and reformats of the coronary arteries for different imaging techniques (5D whole-heart, 4D whole-heart and self-navigated 3D whole-heart imaging) in diastolic phase in one subject. 5D whole-heart images (end-expiratory phase) achieved improved visual delineation of the myocardial wall and different segments of the coronary arteries (white arrows) over 4D whole-heart images, and improved delineation of the LAD over self-navigated 3D whole-heart images. Comparison of the systolic phase from this subject is shown in the Supporting Materials (Figure S2), where 5D whole-heart images shows similar improvement. Figure 6b shows the corresponding respiratory motion pattern extracted from the continuous acquired whole-heart dataset in this subject.

Figure 7a shows the same comparison as in one volunteer with deep breathing pattern during data acquisition. In this subject, motion-related blurring was found in both 3D and 4D images with poor visualization of the coronary arteries. In contrast, the 5D whole-heart images showed adequate image quality, with far greater segmental visualization of the coronary arteries. Figure 7b shows the corresponding deep and irregular respiratory motion pattern extracted from the continuous acquired whole-heart dataset in this subject.

Figure 8 shows comparison of ECG-triggered and navigator-gated free-breathing 3D Cartesian whole-heart images with 5D whole-heart images in two subjects. While the visualization of the RCA is comparable between both techniques, the delineation of the LAD, particularly for the side branches, is still better in the navigator-gated 3D results. Meanwhile, despite reduced visual noise level, the 5D images suffer from certain loss of details due to sparse regularization. However, 5D whole-heart images shows improvement of overall image quality in the myocardium and great vessels with less artifacts.

Figure 9 shows the comparison of ESV, EDV and EF between 5D whole-heart imaging and breath-held, ECG-gated multislice 2D cardiac cine imaging. Corresponding Bland-Altman analysis in the Supporting Materials (Figure S3) suggested good agreement for quantification of cardiac function. The mean differences of 5D whole-heart v.s. 2D cine for ESV, EDV and EF were 3.3 ml, 1.1 ml and −2.0%, respectively.

Discussion

MRI is regarded as the only single modality that can achieve a comprehensive cardiac imaging examination, including assessment of ventricular function, myocardial perfusion and viability, cardiovascular anatomy and hemodynamics. However, the overall implementation of cardiac MRI into clinical practice has been relatively slow, largely due to constraints on MR imaging speed and the influence of physiologic motion. In order to

optimize clinical scan time, breath-hold imaging protocols tailored to answer specific clinical question are usually performed in a sequential fashion, leading to a complex and cumbersome imaging paradigm that requires operator experience and, often, physician supervision. Although various fast imaging approaches, such as parallel imaging (53–55) and compressed sensing (46,56,57), have been applied to accelerate cardiac MR scans (7,11,58–62), they have had relatively little impact in reducing the complexity of imaging workflow. 4D cardiac MRI enables greatly improved scan efficiency with significantly simplified imaging workflow, allowing for assessment of cardiac function and whole-heart anatomy at different cardiac phases (20,22,23). However, respiratory motion can still be a significant challenge, particularly for patients with deep breathing.

In this work, we proposed a 5D cardiac and respiratory motion-resolved whole-heart sparse MRI framework employing a single continuous data acquisition and reconstruction of anatomical and functional information without the need for motion correction. The 5D imaging approach combines a continuous 3D golden-angle radial sampling scheme with a multidimensional compressed sensing technique for reconstruction of separated cardiac and respiratory dimensions with high spatial resolution (1.15 mm isotropic) and temporal resolution (~40–50 ms per cardiac phase). It requires no patient co-operation beyond lying generally still, no planning of scan planes or tailoring to the ECG trace, and no motion correction during image acquisition and reconstruction. It can be completed in about 14 minutes without contrast injection and can provide both functional and anatomical information with not merely corrected but actively resolved cardiac and respiratory motion in a single continuous MR scan.

The performance of 5D whole-heart MRI was compared against 3D and 4D whole-heart MRI with translational respiratory motion correction in a first volunteer study. Our results showed that 5D whole-heart MRI achieved better delineation of whole-heart anatomy, including both myocardium and assorted vessels. It also achieved higher vessel sharpness in coronary arteries, suggesting that less vessel blurring and thus better vessel contrast can be obtained. More importantly, since respiratory motion correction was not required in the 5D whole-heart MRI, it can be more robust to deep breathing.

The proposed 5D sparse cardiac imaging framework can be combined with various golden-angle sampling schemes in both radial and Cartesian trajectory (20,22,63–65). Golden-angle sampling pattern ensures continuous k-space coverage and offers the possibility of quasi-arbitrary retrospective data sorting with approximately uniform k-space coverage. In this work, we chose to evaluate our framework using a 3D golden-angle radial b-SSFP sequence since this combination would deliver a new simple and motion-robust whole-heart MRI framework without the need of contrast media, thus further simplifying patient preparation and avoiding the side-effect of contrast injection.

The current implementation of the 5D whole-heart MRI framework has several limitations that warrant discussion. First, a continuous b-SSFP data acquisition is associated with increased SAR and compromised performance in fat suppression. The need to periodically employ fat saturation module, together with additional ramp-up pulses after that for restoring a steady-state, in turn led to a long scan time (~14 min). In addition, such a data

acquisition scheme also resulted in acquisition of self-navigation spokes every ~150 ms (fat saturation pulse, 10 ramp pulses and the 22 spokes in each interleave as shown in Figure 1a), making it challenging for self-navigation of cardiac motion. A possible solution to solve these problems is to switch the RF excitation to frequency selective excitation (e.g., water-excitation), and to acquire the self-navigation spokes more frequently, as proposed by Pang et al in (20). This can allow maintenance of true steady-state during the entire scan, detection of cardiac motion signal from acquired k-space data, and improved fat saturation. It can also enable reduced SAR by eliminating fat saturation and ramp-up pulses. Implementation of 5D whole-heart MRI framework with such sampling schemes is currently under development, and its extension with other novel sampling strategies will also be explored more in future work. Second, the current sequence demands relatively long image reconstruction times, which is partly due to increased image dimensionality as well as the preliminary implementation of reconstruction algorithm in MATLAB, which was intended to show feasibility of the proposed technique. Once the value of our new whole-heart imaging approach is demonstrated, further and dedicated efforts will be directed towards translate this technique for clinical utilization. Moreover, different solutions, such as the Gadgetron and Yarra framework (66,67), have already been proposed towards clinical use of highly computationally demanding reconstruction techniques. These can be further incorporated into our future implementation. Third, the reconstructed 5D images contain substantial dynamic information. Thus, it is desirable to develop a software tool that can flexibly extract useful information to answer specific clinical questions, particularly for measurement of cardiac function (68).

It is another limitation of our work that 5D whole-heart imaging was only compared with 4D and 3D whole-heart imaging with 1D translational motion correction. Although 1D translational motion correction has been previously tested in both patient and volunteer studies in our center (25,27,43), additional comparison with other respiratory motion correction schemes, such as 3D affine or non-rigid motion correction, would be necessary to further validate the value of the proposed framework. On the other hand, 3D motion correction and motion-resolved reconstruction are complementary techniques that could be combined to further increase motion robustness (69). In addition, conventional ECG-triggered and navigator-gated 3D Cartesian images was performed in two subjects only. In the next step, it would be necessary fully evaluate the clinical utility of this framework in patient study by comparing with conventional reference approach, and to test whether the 5D imaging approach can enable better visualization of more distal coronary arteries and the left circumflex artery (LCX), both of which have traditionally been challenging to image. Our first patient studies, including evaluation of the RCA, LAD and LCX, are currently underway and preliminary results have already been reported in (70).

In addition to assessment of myocardial function, great vessels and the coronary arteries, the proposed 5D whole-heart MRI framework can also be extended to other cardiac MR applications such as myocardial parameter mapping (71,72) or 4D flow imaging (73). As recently shown in (72), additional dimensions provide extra correlations that can be exploited to further improve the performance of sparse image reconstruction. Moreover, these different types of cardiac scans may be potentially combined as a synergistic free-breathing whole-heart imaging framework that can enable the ultimate goal of “one-stop-

shopping" comprehensive examination of the cardiovascular system, with diverse information streaming in continuously. Such an imaging and reconstruction strategy entails more than just acceleration of existing imaging protocols, and it could facilitate a shift of the day-to-day clinical workflow from conventional time-consuming and tailored acquisitions of carefully targeted slabs towards rapid, continuous and comprehensive volumetric acquisitions, with user-defined reconstructions that can be adapted retrospectively for different clinical needs (74). It would then have the potential to change the entire experience of cardiac MRI for physicians, for technologists and for patients.

Conclusion

The 5D whole-heart sparse MRI framework developed in this work enables easy-to-use free-breathing cardiac and respiratory motion-resolved whole-heart MR imaging at high spatial and temporal resolution using a multidimensional compressed sensing technique. Instead of removing motion corrupted data measurements or correcting for motion, 5D whole-heart images containing separated cardiac and respiratory motion dimensions are reconstructed, allowing for assessment of myocardial function in arbitrary orientation and visualization of high resolution coronary arteries at multiple cardiac phases without the need for motion correction. This imaging framework has the potential to enable simplification of MRI workflow and increase the utilization, efficiency and efficacy of cardiac MR examinations.

Supplementary Material

Refer to Web version on PubMed Central for supplementary material.

Acknowledgments

This work was supported in part by the NIH and Swiss National Science Foundation, and was performed under the rubric of the Center for Advanced Imaging Innovation and Research (CAI^2R), a NIBIB Biomedical Technology Resource Center (NIH P41 EB017183). Early support was also derived from NIH R01 EB000447. The authors would like to thank Dr. Florian Knoll at NYU School of Medicine for providing the gpuNUFFT toolbox (http://www.ismrm.org/MR-Hub/).

References

1. Pennell DJ. Cardiovascular magnetic resonance. Circulation. 2010; 121(5):692–705. [PubMed: 20142462]
2. Bluemke DA, Achenbach S, Budoff M, Gerber TC, Gersh B, Hillis LD, Hundley WG, Manning WJ, Printz BF, Stuber M, Woodard PK. Noninvasive coronary artery imaging: magnetic resonance angiography and multidetector computed tomography angiography: a scientific statement from the american heart association committee on cardiovascular imaging and intervention of the council on cardiovascular radiology and intervention, and the councils on clinical cardiology and cardiovascular disease in the young. Circulation. 2008; 118(5):586–606. [PubMed: 18586979]
3. Stuber M, Weiss RG. Coronary magnetic resonance angiography. Journal of magnetic resonance imaging : JMRI. 2007; 26(2):219–234. [PubMed: 17610288]
4. Bloomgarden DC, Fayad ZA, Ferrari VA, Chin B, Sutton MG, Axel L. Global cardiac function using fast breath-hold MRI: validation of new acquisition and analysis techniques. Magnetic resonance in medicine. 1997; 37(5):683–692. [PubMed: 9126942]
5. Bluemke DA, Boxerman JL, Atalar E, McVeigh ER. Segmented K-space cine breath-hold cardiovascular MR imaging: Part 1. Principles and technique. AJR American journal of roentgenology. 1997; 169(2):395–400. [PubMed: 9242742]

6. McVeigh ER. MRI of myocardial function: motion tracking techniques. Magnetic resonance imaging. 1996; 14(2):137–150. [PubMed: 8847969]
7. Vincenti G, Monney P, Chaptinel J, Rutz T, Coppo S, Zenge MO, Schmidt M, Nadar MS, Piccini D, Chevre P, Stuber M, Schwitter J. Compressed sensing single-breath-hold CMR for fast quantification of LV function, volumes, and mass. JACC Cardiovasc Imaging. 2014; 7(9):882–892. [PubMed: 25129517]
8. Plein S, Ridgway JP, Jones TR, Bloomer TN, Sivananthan MU. Coronary artery disease: assessment with a comprehensive MR imaging protocol--initial results. Radiology. 2002; 225(1):300–307. [PubMed: 12355020]
9. Foo TK, Ho VB, Saranathan M, Cheng LQ, Sakuma H, Kraitchman DL, Wu KC, Bluemke DA. Feasibility of integrating high-spatial-resolution 3D breath-hold coronary MR angiography with myocardial perfusion and viability examinations. Radiology. 2005; 235(3):1025–1030. [PubMed: 15914483]
10. Gutberlet M, Noeske R, Schwinge K, Freyhardt P, Felix R, Niendorf T. Comprehensive cardiac magnetic resonance imaging at 3.0 Tesla: feasibility and implications for clinical applications. Investigative radiology. 2006; 41(2):154–167. [PubMed: 16428987]
11. Xu J, Kim D, Otazo R, Srichai MB, Lim RP, Axel L, McGorty KA, Niendorf T, Sodickson DK. Towards a five-minute comprehensive cardiac MR examination using highly accelerated parallel imaging with a 32-element coil array: feasibility and initial comparative evaluation. Journal of magnetic resonance imaging : JMRI. 2013; 38(1):180–188. [PubMed: 23197471]
12. Li D, Paschal CB, Haacke EM, Adler LP. Coronary arteries: three-dimensional MR imaging with fat saturation and magnetization transfer contrast. Radiology. 1993; 187(2):401–406. [PubMed: 8475281]
13. Park J, Larson AC, Zhang Q, Simonetti O, Li D. 4D radial coronary artery imaging within a single breath-hold: cine angiography with phase-sensitive fat suppression (CAPS). Magnetic resonance in medicine. 2005; 54(4):833–840. [PubMed: 16149060]
14. Gharib AM, Herzka DA, Ustun AO, Desai MY, Locklin J, Pettigrew RI, Stuber M. Coronary MR angiography at 3T during diastole and systole. Journal of magnetic resonance imaging : JMRI. 2007; 26(4):921–926. [PubMed: 17896391]
15. Kressler B, Spincemaille P, Nguyen TD, Cheng L, Xi Hai Z, Prince MR, Wang Y. Three-dimensional cine imaging using variable-density spiral trajectories and SSFP with application to coronary artery angiography. Magnetic resonance in medicine. 2007; 58(3):535–543. [PubMed: 17763360]
16. Lai P, Huang F, Larson AC, Li D. Fast four-dimensional coronary MR angiography with k-t GRAPPA. Journal of magnetic resonance imaging : JMRI. 2008; 27(3):659–665. [PubMed: 18224671]
17. Lai P, Larson AC, Park J, Carr JC, Li D. Respiratory self-gated four-dimensional coronary MR angiography: a feasibility study. Magnetic resonance in medicine. 2008; 59(6):1378–1385. [PubMed: 18506786]
18. Liu J, Spincemaille P, Codella NC, Nguyen TD, Prince MR, Wang Y. Respiratory and cardiac self-gated free-breathing cardiac CINE imaging with multiecho 3D hybrid radial SSFP acquisition. Magnetic resonance in medicine. 2010; 63(5):1230–1237. [PubMed: 20432294]
19. Wu HH, Gurney PT, Hu BS, Nishimura DG, McConnell MV. Free-breathing multiphase whole-heart coronary MR angiography using image-based navigators and three-dimensional cones imaging. Magnetic resonance in medicine. 2013; 69(4):1083–1093. [PubMed: 22648856]
20. Pang J, Sharif B, Fan Z, Bi X, Arsanjani R, Berman DS, Li D. ECG and navigator-free four-dimensional whole-heart coronary MRA for simultaneous visualization of cardiac anatomy and function. Magnetic resonance in medicine. 2014; 72(5):1208–1217. [PubMed: 25216287]
21. Liu J, Nguyen TD, Zhu Y, Spincemaille P, Prince MR, Weinsaft JW, Saloner D, Wang Y. Self-gated free-breathing 3D coronary CINE imaging with simultaneous water and fat visualization. PloS one. 2014; 9(2):e89315. [PubMed: 24586682]
22. Coppo S, Piccini D, Bonanno G, Chaptinel J, Vincenti G, Feliciano H, van Heeswijk RB, Schwitter J, Stuber M. Free-running 4D whole-heart self-navigated golden angle MRI: Initial results. Magnetic resonance in medicine. 2015; 74(5):1306–1316. [PubMed: 25376772]

23. Han F, Rapacchi S, Khan S, Ayad I, Salusky I, Gabriel S, Plotnik A, Finn JP, Hu P. Four-dimensional, multiphase, steady-state imaging with contrast enhancement (MUSIC) in the heart: a feasibility study in children. Magnetic resonance in medicine. 2015; 74(4):1042–1049. [PubMed: 25302932]
24. Stehning C, Bornert P, Nehrke K, Eggers H, Stuber M. Free-breathing whole-heart coronary MRA with 3D radial SSFP and self-navigated image reconstruction. Magnetic resonance in medicine. 2005; 54(2):476–480. [PubMed: 16032682]
25. Piccini D, Littmann A, Nielles-Vallespin S, Zenge MO. Respiratory self-navigation for whole-heart bright-blood coronary MRI: methods for robust isolation and automatic segmentation of the blood pool. Magnetic resonance in medicine. 2012; 68(2):571–579. [PubMed: 22213169]
26. Henningsson M, Koken P, Stehning C, Razavi R, Prieto C, Botnar RM. Whole-heart coronary MR angiography with 2D self-navigated image reconstruction. Magnetic resonance in medicine. 2012; 67(2):437–445. [PubMed: 21656563]
27. Piccini D, Monney P, Sierro C, Coppo S, Bonanno G, van Heeswijk RB, Chaptinel J, Vincenti G, de Blois J, Koestner SC, Rutz T, Littmann A, Zenge MO, Schwitter J, Stuber M. Respiratory self-navigated postcontrast whole-heart coronary MR angiography: initial experience in patients. Radiology. 2014; 270(2):378–386. [PubMed: 24471387]
28. Ginami G, Bonanno G, Schwitter J, Stuber M, Piccini D. An iterative approach to respiratory self-navigated whole-heart coronary MRA significantly improves image quality in a preliminary patient study. Magnetic resonance in medicine. 2016; 75(4):1594–1604. [PubMed: 25960337]
29. Bonanno G, Puy G, Wiaux Y, van Heeswijk RB, Piccini D, Stuber M. Self-navigation with compressed sensing for 2D translational motion correction in free-breathing coronary MRI: a feasibility study. PloS one. 2014; 9(8):e105523. [PubMed: 25171369]
30. Bhat H, Ge L, Nielles-Vallespin S, Zuehlsdorff S, Li D. 3D radial sampling and 3D affine transform-based respiratory motion correction technique for free-breathing whole-heart coronary MRA with 100% imaging efficiency. Magnetic resonance in medicine. 2011; 65(5):1269–1277. [PubMed: 21500255]
31. Pang J, Bhat H, Sharif B, Fan Z, Thomson LE, LaBounty T, Friedman JD, Min J, Berman DS, Li D. Whole-heart coronary MRA with 100% respiratory gating efficiency: self-navigated three-dimensional retrospective image-based motion correction (TRIM). Magnetic resonance in medicine. 2014; 71(1):67–74. [PubMed: 23401157]
32. Henningsson M, Prieto C, Chiribiri A, Vaillant G, Razavi R, Botnar RM. Whole-heart coronary MRA with 3D affine motion correction using 3D image-based navigation. Magnetic resonance in medicine. 2014; 71(1):173–181. [PubMed: 23400902]
33. Aitken AP, Henningsson M, Botnar RM, Schaeffter T, Prieto C. 100% Efficient three-dimensional coronary MR angiography with two-dimensional beat-to-beat translational and bin-to-bin affine motion correction. Magnetic resonance in medicine. 2015; 74(3):756–764. [PubMed: 25236813]
34. Bonanno, G., Piccini, D., Marechal, B., Zenge, M., Stuber, M. A New Binning Approach for 3D Motion Corrected Self-Navigated Whole-Heart Coronary MRA Using Independent Component Analysis of Individual Coils. Proceedings of the 22nd Annual Meeting of ISMRM; Milan, Italy. 2014; p. 936
35. Ingle RR, Wu HH, Addy NO, Cheng JY, Yang PC, Hu BS, Nishimura DG. Nonrigid autofocus motion correction for coronary MR angiography with a 3D cones trajectory. Magnetic resonance in medicine. 2014; 72(2):347–361. [PubMed: 24006292]
36. Feng L, Axel L, Chandarana H, Block KT, Sodickson DK, Otazo R. XD-GRASP: Golden-angle radial MRI with reconstruction of extra motion-state dimensions using compressed sensing. Magnetic resonance in medicine. 2016; 75(2):775–788. [PubMed: 25809847]
37. Axel L, Otazo R. Accelerated MRI for the assessment of cardiac function. The British journal of radiology. 2016 20150655.
38. Chandarana H, Feng L, Ream J, Wang A, Babb JS, Block KT, Sodickson DK, Otazo R. Respiratory Motion-Resolved Compressed Sensing Reconstruction of Free-Breathing Radial Acquisition for Dynamic Liver Magnetic Resonance Imaging. Investigative radiology. 2015; 50(11):749–756. [PubMed: 26146869]

39. Piccini D, Feng L, Bonanno G, Coppo S, Yerly J, Lim RP, Schwitter J, Sodickson DK, Otazo R, Stuber M. Four-dimensional respiratory motion-resolved whole heart coronary MR angiography. Magnetic resonance in medicine. 2016; Early View. doi: 10.1002/mrm.26221
40. Feng, L., Axel, L., Latson, AL., Xu, J., Sodickson, DK., Otazo, R. Compressed sensing with synchronized cardiorespiratory sparsity for free-breathing cine MRI: initial comparative study on patients with arrhythmias. Proceedings of the 17th Annual SCMR Scientific Sessions; New Orleans, LA, USA. 2014; p. O17
41. Piekarski E, Chitiboi T, Ramb R, Feng L, Axel L. Use of self-gated radial cardiovascular magnetic resonance to detect and classify arrhythmias (atrial fibrillation and premature ventricular contraction). J Cardiovasc Magn Reson. 2016; 18(1):83. [PubMed: 27884152]
42. Piccini D, Littmann A, Nielles-Vallespin S, Zenge MO. Spiral phyllotaxis: the natural way to construct a 3D radial trajectory in MRI. Magnetic resonance in medicine. 2011; 66(4):1049–1056. [PubMed: 21469185]
43. Monney P, Piccini D, Rutz T, Vincenti G, Coppo S, Koestner SC, Sekarski N, Di Bernardo S, Bouchardy J, Stuber M, Schwitter J. Single centre experience of the application of self navigated 3D whole heart cardiovascular magnetic resonance for the assessment of cardiac anatomy in congenital heart disease. J Cardiovasc Magn Reson. 2015; 17:55. [PubMed: 26156377]
44. Sakuma H, Ichikawa Y, Suzawa N, Hirano T, Makino K, Koyama N, Van Cauteren M, Takeda K. Assessment of coronary arteries with total study time of less than 30 minutes by using whole-heart coronary MR angiography. Radiology. 2005; 237(1):316–321. [PubMed: 16126921]
45. Setser RM, Fischer SE, Lorenz CH. Quantification of left ventricular function with magnetic resonance images acquired in real time. Journal of magnetic resonance imaging : JMRI. 2000; 12(3):430–438. [PubMed: 10992310]
46. Lustig M, Donoho D, Pauly JM. Sparse MRI: The application of compressed sensing for rapid MR imaging. Magnetic resonance in medicine. 2007; 58(6):1182–1195. [PubMed: 17969013]
47. Feng L, Grimm R, Block KT, Chandarana H, Kim S, Xu J, Axel L, Sodickson DK, Otazo R. Golden-angle radial sparse parallel MRI: combination of compressed sensing, parallel imaging, and golden-angle radial sampling for fast and flexible dynamic volumetric MRI. Magnetic resonance in medicine. 2014; 72(3):707–717. [PubMed: 24142845]
48. Walsh DO, Gmitro AF, Marcellin MW. Adaptive reconstruction of phased array MR imagery. Magnetic resonance in medicine. 2000; 43(5):682–690. [PubMed: 10800033]
49. Knoll, F., Schwarzl, A., Diwoky, C., Sodickson, DK. gpuNUFFT - An Open Source GPU Library for 3D Regridding with Direct MATLAB Interface. Proceedings of the 22nd Annual Meeting of ISMRM; Milan, Italy. 2014; p. 4297
50. Coppo, S., Feng, LDP., Chaptinel, JGB., Vincenti, G., Schwitter, J., Otazo, R., Sodickson, DK., Stuber, M. Improved Free-Running Self-Navigated 4D Whole-Heart MRI Through Combination of Compressed Sensing and Parallel Imaging. Proceedings of the 23rd Annual Meeting of ISMRM; Toronto, Canada. 2015; p. 28
51. Austen WG, Edwards JE, Frye RL, Gensini GG, Gott VL, Griffith LS, McGoon DC, Murphy ML, Roe BB. A reporting system on patients evaluated for coronary artery disease. Report of the Ad Hoc Committee for Grading of Coronary Artery Disease, Council on Cardiovascular Surgery, American Heart Association. Circulation. 1975; 51(4 Suppl):5–40. [PubMed: 1116248]
52. Etienne A, Botnar RM, Van Muiswinkel AM, Boesiger P, Manning WJ, Stuber M. “Soap-Bubble” visualization and quantitative analysis of 3D coronary magnetic resonance angiograms. Magnetic resonance in medicine. 2002; 48(4):658–666. [PubMed: 12353283]
53. Sodickson DK, Manning WJ. Simultaneous acquisition of spatial harmonics (SMASH): fast imaging with radiofrequency coil arrays. Magnetic resonance in medicine. 1997; 38(4):591–603. [PubMed: 9324327]
54. Pruessmann KP, Weiger M, Scheidegger MB, Boesiger P. SENSE: sensitivity encoding for fast MRI. Magnetic resonance in medicine. 1999; 42(5):952–962. [PubMed: 10542355]
55. Griswold MA, Jakob PM, Heidemann RM, Nittka M, Jellus V, Wang J, Kiefer B, Haase A. Generalized autocalibrating partially parallel acquisitions (GRAPPA). Magnetic resonance in medicine. 2002; 47(6):1202–1210. [PubMed: 12111967]

56. Lustig M, Pauly JM. SPIRiT: Iterative self-consistent parallel imaging reconstruction from arbitrary k-space. Magnetic resonance in medicine. 2010; 64(2):457–471. [PubMed: 20665790]
57. Otazo R, Kim D, Axel L, Sodickson DK. Combination of compressed sensing and parallel imaging for highly accelerated first-pass cardiac perfusion MRI. Magnetic resonance in medicine. 2010; 64(3):767–776. [PubMed: 20535813]
58. Gamper U, Boesiger P, Kozerke S. Compressed sensing in dynamic MRI. Magnetic resonance in medicine. 2008; 59(2):365–373. [PubMed: 18228595]
59. Feng L, Otazo R, Jung H, Jensen JH, Ye JC, Sodickson DK, Kim D. Accelerated cardiac T2 mapping using breath-hold multiecho fast spin-echo pulse sequence with k-t FOCUSS. Magnetic resonance in medicine. 2011; 65(6):1661–1669. [PubMed: 21360737]
60. Feng L, Srichai MB, Lim RP, Harrison A, King W, Adluru G, Dibella EV, Sodickson DK, Otazo R, Kim D. Highly accelerated real-time cardiac cine MRI using k-t SPARSE-SENSE. Magnetic resonance in medicine. 2013; 70(1):64–74. [PubMed: 22887290]
61. Akcakaya M, Basha TA, Pflugi S, Foppa M, Kissinger KV, Hauser TH, Nezafat R. Localized spatio-temporal constraints for accelerated CMR perfusion. Magnetic resonance in medicine. 2014; 72(3):629–639. [PubMed: 24123058]
62. Usman M, Prieto C, Schaeffter T, Batchelor PG. k-t Group sparse: a method for accelerating dynamic MRI. Magnetic resonance in medicine. 2011; 66(4):1163–1176. [PubMed: 21394781]
63. Cheng JY, Zhang T, Ruangwattanapaisarn N, Alley MT, Uecker M, Pauly JM, Lustig M, Vasanawala SS. Free-breathing pediatric MRI with nonrigid motion correction and acceleration. Journal of magnetic resonance imaging : JMRI. 2015; 42(2):407–420. [PubMed: 25329325]
64. Liu J, Saloner D. Accelerated MRI with CIRcular Cartesian UnderSampling (CIRCUS): a variable density Cartesian sampling strategy for compressed sensing and parallel imaging. Quantitative imaging in medicine and surgery. 2014; 4(1):57–67. [PubMed: 24649436]
65. Prieto C, Doneva M, Usman M, Henningsson M, Greil G, Schaeffter T, Botnar RM. Highly efficient respiratory motion compensated free-breathing coronary MRA using golden-step Cartesian acquisition. Journal of magnetic resonance imaging : JMRI. 2015; 41(3):738–746. [PubMed: 24573992]
66. Hansen MS, Sorensen TS. Gadgetron: an open source framework for medical image reconstruction. Magnetic resonance in medicine. 2013; 69(6):1768–1776. [PubMed: 22791598]
67. Block, KT., Grimm, G., Feng, L., Otazo, R., Chandarana, H., Bruno, M., Geppert, C., Sodickson, DK. Bringing Compressed Sensing to Clinical Reality: Prototypic Setup for Evaluation in Routine Applications. Proceedings of the 21st Annual Meeting of ISMRM; Salt Lake City. 2013; p. 3809
68. Chen, Y., Pang, J., Neiman, D., Xie, Y., Nguyen, C., Zhou, Z., Li, D. Automatic Ventricular Function Measurement with Free-Breathing Self-Gated 4D Whole-Heart Cardiac MRI. Proceedings of the 24nd Annual Meeting of ISMRM; Singapore. 2016; p. 2629
69. Cruz G, Atkinson D, Buerger C, Schaeffter T, Prieto C. Accelerated motion corrected three-dimensional abdominal MRI using total variation regularized SENSE reconstruction. Magnetic resonance in medicine. 2016; 75(4):1484–1498. [PubMed: 25996443]
70. Ginami, G., Coppo, S., Feng, L., Piccini, D., Rutz, T., Otazo, R., Sodickson, DK., Stuber, M., Yerly, J. Cardiac and Respiratory Motion-Resolved Free-Running Whole-Heart Coronary MRA of Patients Using 5D XD-GRASP Reconstruction. Proceedings of the 24nd Annual Meeting of ISMRM; Singapore. 2016; p. 2682
71. van Heeswijk RB, Piccini D, Feliciano H, Hullin R, Schwitter J, Stuber M. Self-navigated isotropic three-dimensional cardiac T2 mapping. Magnetic resonance in medicine. 2015; 73(4):1549–1554. [PubMed: 24809849]
72. Christodoulou, A., Shaw, J., Sharif, B., Li, D. A general low-rank tensor framework for high-dimensional cardiac imaging: Application to time-resolved T1 mapping. Proceedings of the 24nd Annual Meeting of ISMRM; Singapore. 2016; p. 867
73. Cheng, J., Zhang, T., Alley, M., Lustig, M., Pauly, J., Vasanawala, S. Ultra-High-Dimensional Flow Imaging (N-D Flow). Proceedings of the 24nd Annual Meeting of ISMRM; Singapore. 2016; p. 325
74. Sodickson, DK., Feng, L., Knoll, F., Cloos, M., Ben-Elibzer, N., Axelsson, A., Chandarana, H., Block, KT., Otazo, R. The rapid imaging renaissance: sparser samples, denser dimensions, and

glimmerings of a grand unified tomography; SPIE Medical Imaging; 2015 Mar 19. 94170G-94170G-14

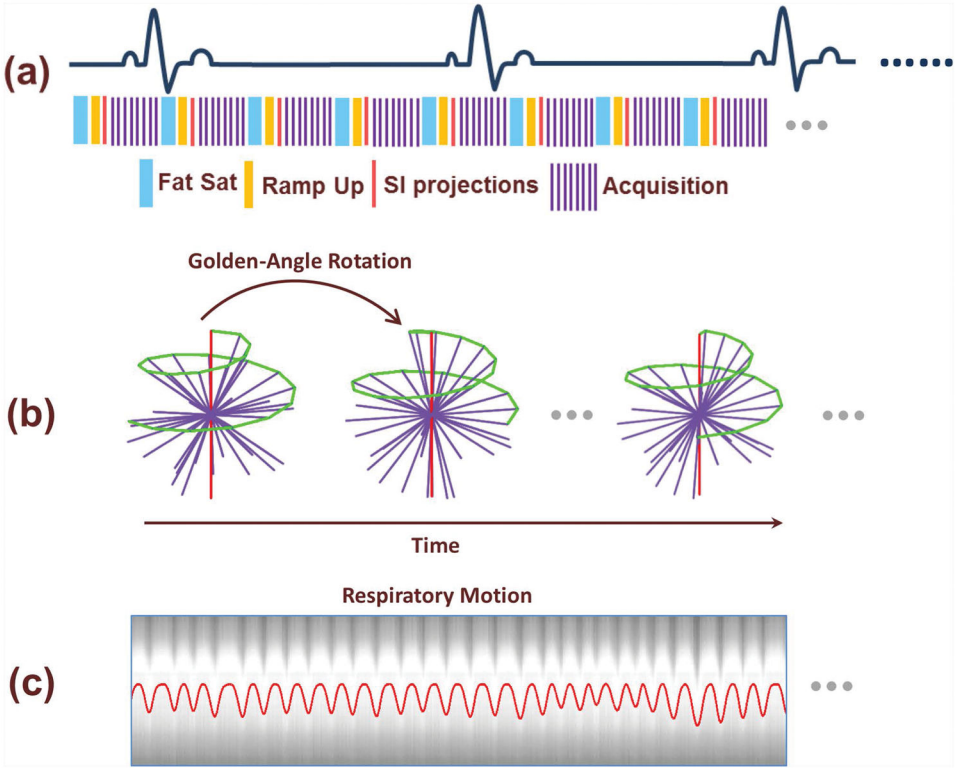

Figure 1.

Data acquisition scheme and respiratory motion extraction for non-ECG-triggered whole-heart imaging. (a) A 3D radial b-SSFP sequence that is segmented into multiple interleaves (purple lines) is employed for MR data acquisition. Each interleave starts with a spoke oriented along the superior to inferior direction for self-navigation (red lines) and is preceded by fat saturation (blue lines). Ten additional ramp-up RF pulses (yellow lines) are deployed between the fat saturation module and the data acquisition window in order to restore restoring steady-state at each interleave. (b) 3D radial sampling trajectory based on the spiral phyllotaxis pattern. Each interleave is rotated by the golden-angle (137.51°) about the z-axis, starting with a self-navigation spoke (red lines) for respiratory motion extraction. (c) An extracted respiratory motion signal is superimposed to the 1D FFT of an example series of SI readouts.

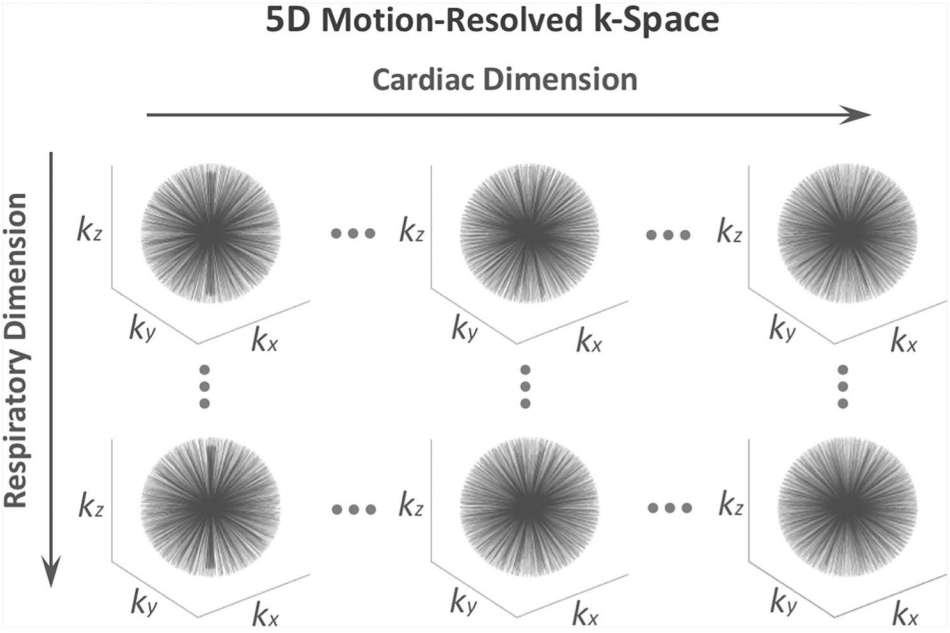

Figure 2.

The acquired k-space is sorted into a 5D dataset (k_x-k_y-k_z-cardiac phase-respiratory phase) using respiratory motion signal extracted from self-navigators and cardiac motion signal obtained from recorded ECG time stamp. The datasets are first binned into different cardiac phases with a desired temporal resolution, then each cardiac phase is further sorted into multiple respiratory motion phases spanning from end-expiration to end-inspiration. The data sorting process is performed such that the number of spokes grouped in each temporal phase is the same.

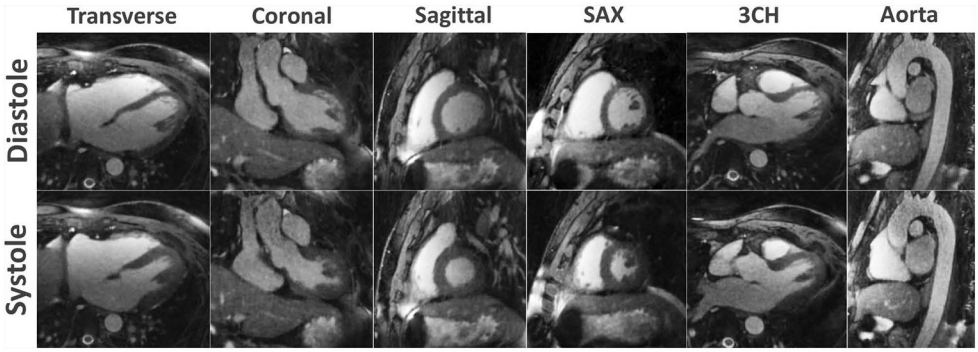

Figure 3.

Slices through the ventricular chambers and the aorta in both diastolic (top) and systolic (bottom) phases, derived from the end-expiratory phase of one representative 5D whole-heart image set. Images can be retrospectively reformatted into any desired orientation for visualization.

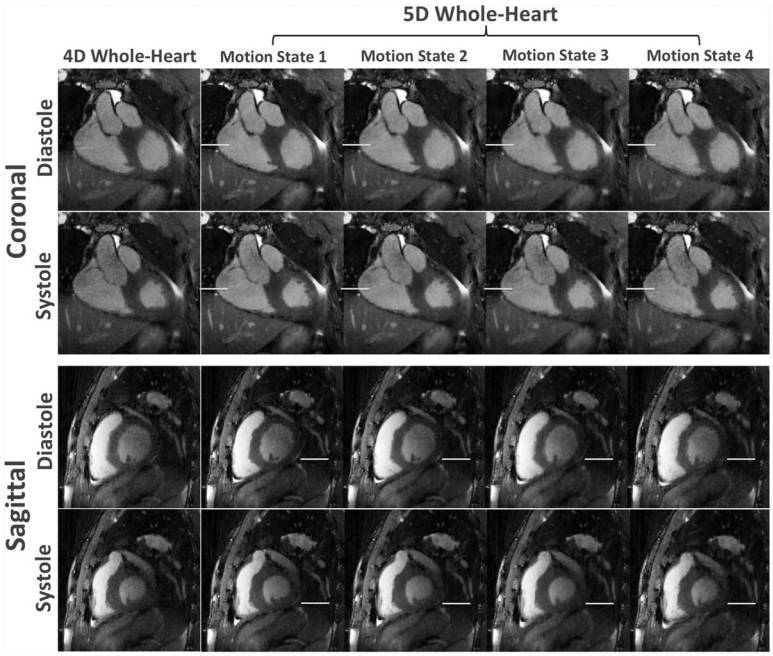

Figure 4.

Comparison of respiratory motion-corrected 4D whole-heart images with 5D whole-heart images in coronal and sagittal planes. White lines overlaid atop the diaphragm in the 5D whole-heart images suggest that respiratory motion can be resolved using the proposed 5D image reconstruction method.

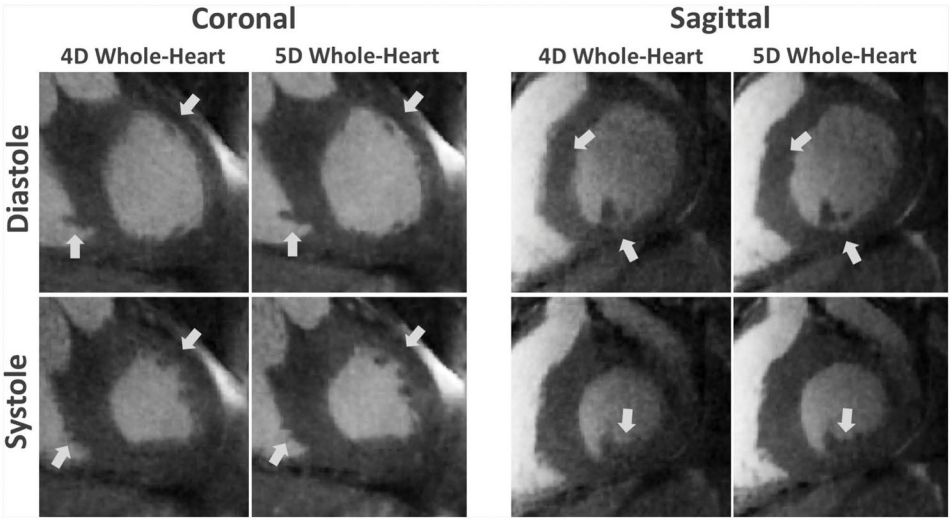

Figure 5.

Zoomed view of the myocardium of the same dataset as shown in Figure 4. Residual respiratory motion blurring can be noticed in the myocardium and papillary muscles of 4D whole-heart images, while 5D whole-heart images achieved better image quality and improved image sharpness, as indicated by the white arrows. The end-expiratory phase is shown for the 5D whole-heart images.

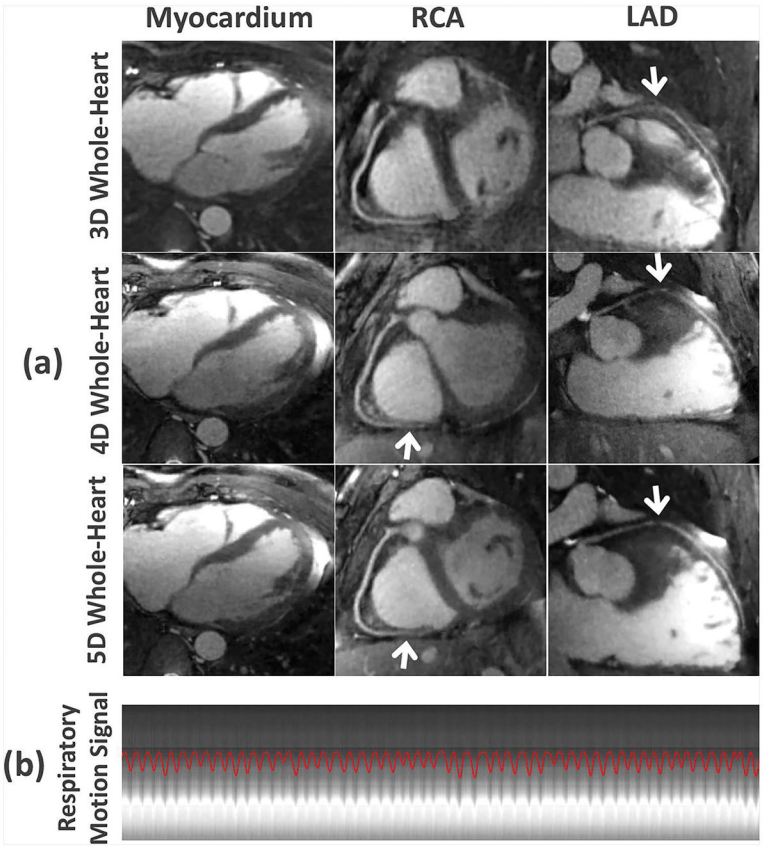

Figure 6.

(a) Comparison of the myocardium, the right (RCA) and left anterior descending (LAD) coronary arteries for different imaging techniques in one subject. 5D whole-heart images (end-expiratory phase) achieved improved visual delineation of the myocardial wall and different segments of the coronary arteries (white arrows) over 4D whole-heart images, and improved delineation of the LAD over self-navigated 3D whole-heart images. (b) Corresponding respiratory motion pattern extracted from the continuous acquired whole-heart dataset in this subject.

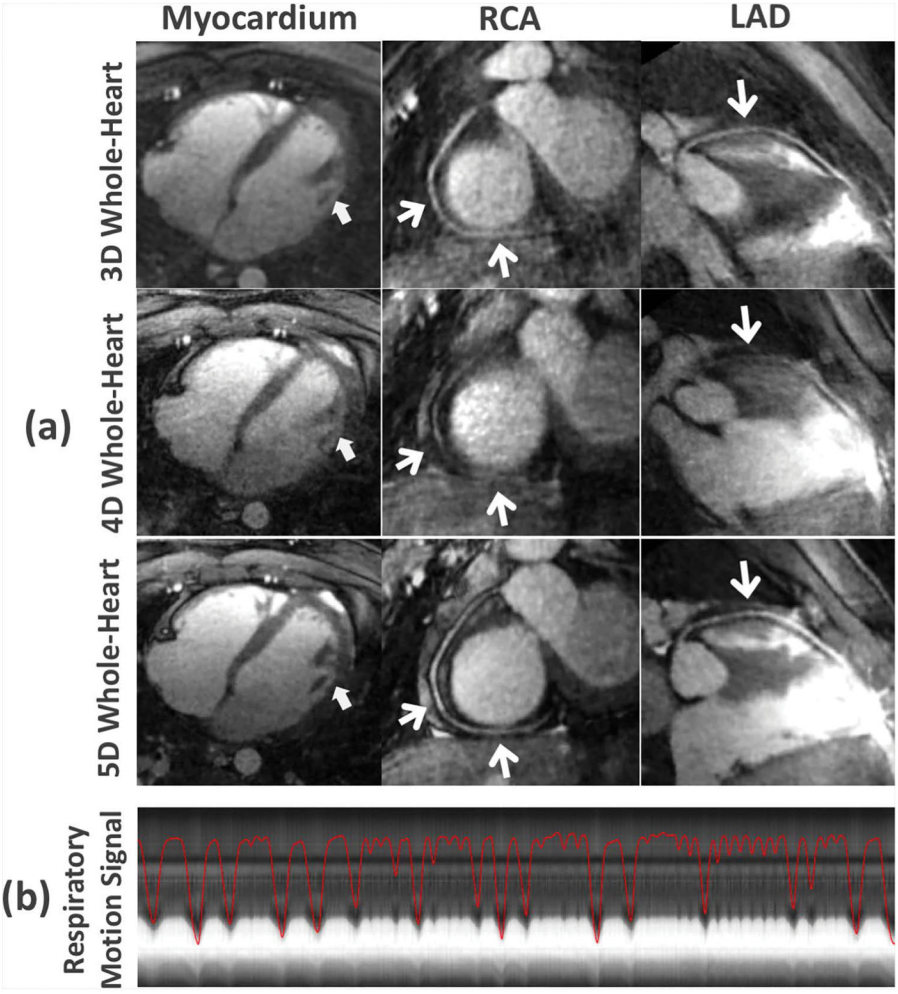

Figure 7.

(a) Comparison of the myocardium, the right (RCA) and left anterior descending (LAD) coronary arteries for different imaging techniques in one subject with deep breathing pattern during data acquisition. Residual motion-induced blurring was seen in both 3D and 4D whole-heart images, while 5D whole-heart images showed better delineation of both the myocardial wall and different segments of the coronary arteries (white arrows). (b) Corresponding deep and irregular respiratory motion pattern of this subject during continuous data acquisition.

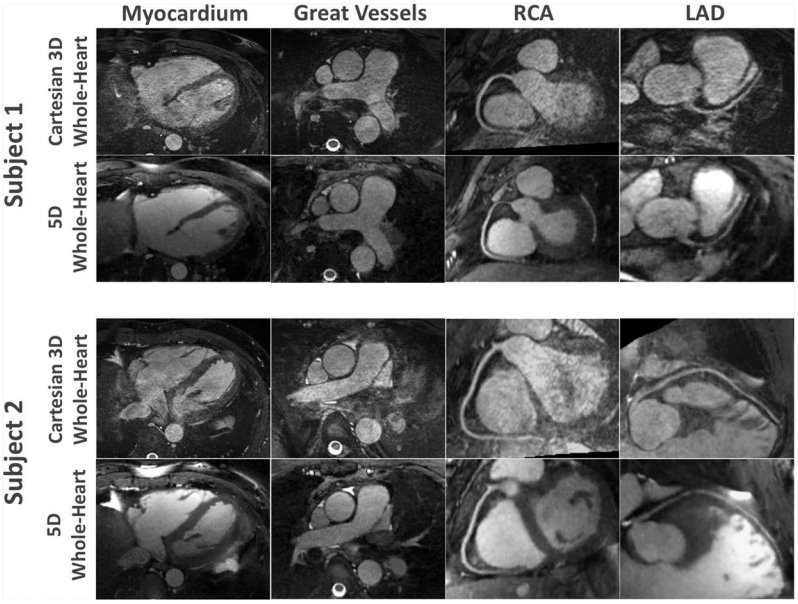

Figure 8.

Comparison of ECG-triggered and navigator-gated free-breathing 3D Cartesian whole-heart images with 5D whole-heart images in two subjects. The visualization of the RCA is comparable between both techniques while the delineation of the LAD is relatively better in the navigator-gated 3D imaging approach. However, the 5D whole-heart images show improvement of overall image quality in the myocardium and great vessels with less noise and artifacts.

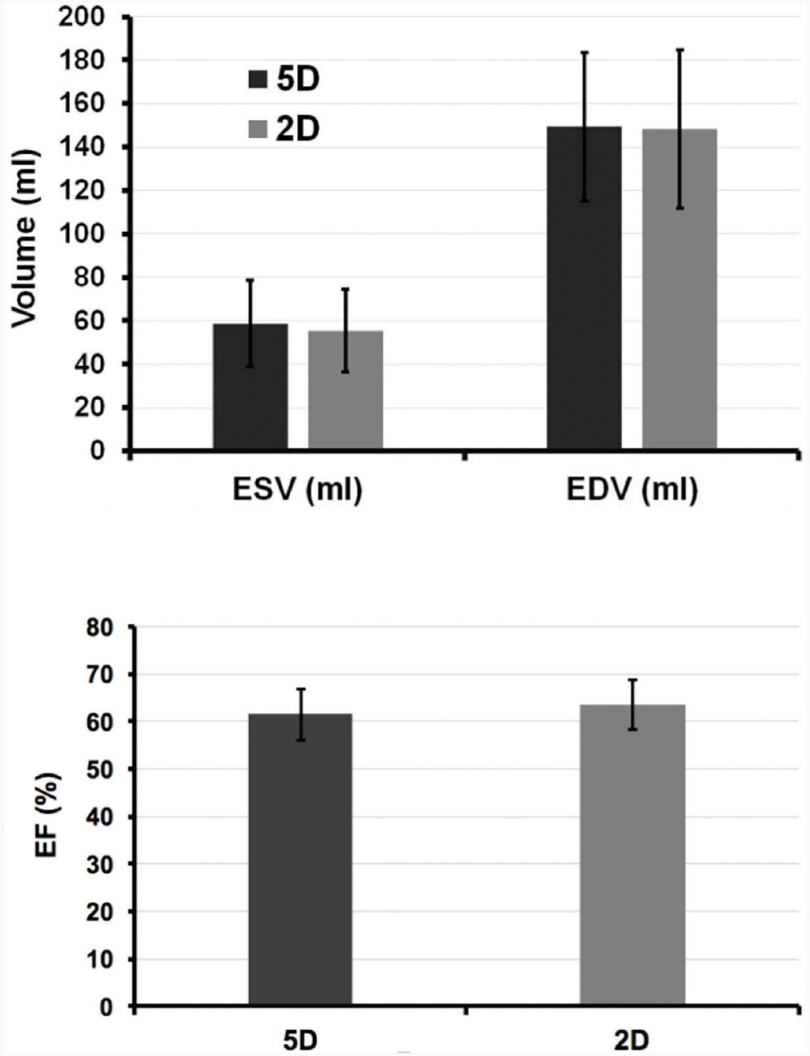

Figure 9.

Comparison of ESV, EDV and EF between 5D whole-heart imaging and breath-held, ECG-gated multislice 2D cardiac cine imaging.

Abbreviations: ESV: End-Systolic Volume; EDV: End-Diastolic Volume; EF: Ejection fraction.

Table 1

(a) Summary of readers' scores for the myocardium, great vessels and coronary arteries. The scores of different great vessels were considered together for each imaging technique, and the scores of different segments of the coronary arteries were considered together for each imaging technique. All the scores were averaged from two readers. A 0–4 scale (0: non-diagnostic, 1: poor, 2: adequate, 3: good, 4: excellent) was used for scoring of the myocardium and great vessels. A different 0–4 scale (0: not visible, 1: markedly blurred, 2: moderately blurred, 3: mildly blurred, 4: sharply defined) was used for scoring of the coronary arteries. Any coronary artery with a grade higher than 0 was considered to be visualized. (b) Summary of measured coronary sharpness and length. The sharpness of proximal and mid segments was considered together on a per-vessel basis for statistical analysis.

(a)

	Diastole			Systole	
	5D Whole-Heart (End Expiration)	**4D Whole-Heart**	**3D Whole-Heart**	**5D Whole-Heart (End Expiration)**	**4D Whole-Heart**
Myocardium	3.2±0.5	2.4±0.9*	2.2±0.6*	2.9±0.5	2.1±0.7*
Asc Aorta + Desc Aorta + MPA + RPA + LPA + SVC	3.4±0.5	2.6±0.9*	2.4±0.6*	3.2±0.6	2.6±0.9*
RCA + LM + LAD	2.6±0.9	1.9±1.0*	2.2±1.0*	2.7±0.7	1.6±1.1*

(b)

Coronary Artery	**Measured Parameter**	Diastole			Systole	
		5D Whole-Heart (End Expiration)	**4D Whole-Heart**	**3D Whole-Heart**	**5D Whole-Heart (End Expiration)**	**4D Whole-Heart**
RCA (proximal + Mid)	Sharpness (%)	46.0 ± 7.3	41.6 ± 9.0*	38.9 ± 14.2*	46.5 ± 9.2	42.7 ± 12.2
LAD (proximal + Mid)	Sharpness (%)	42.2 ± 6.6	37.5 ± 7.0*	34.1 ±7.0*	42.5 ± 9.6	38.5 ± 9.4*
RCA	Length (mm)	101.5 ± 30.8	86.2 ± 29.7	90.9 ± 29.9*	88.3 ± 31.0	68.2 ± 32.5
LM+LAD	Length (mm)	92.6 ± 35.7	86.1 ± 34.9	93.3 ± 36.5	84.0 ± 34.2	70.0 ± 35.5*

Abbreviations: Asc Aorta: ascending aorta; Desc Aorta: descending aorta; MPA: main pulmonary artery; RPA: right pulmonary arteries; LPA: left pulmonary arteries; SVC: superior vena cava (SVC); RCA: right coronary artery; LAD: left anterior descending artery; LM: left main stem.

* indicates statistical significance compared with 5D whole-heart MRI.